Powder Synthesis and Sintering

DEPOSITION OF PLATINUM NANOPARTICLES ONTO COPPER FOILS BY ELECTROPHORESIS: A STUDY OF THE SINTERING DYNAMICS AT THE PLATINUM-COPPER INTERFACE

Deborah C. Blaine*, Alexander Ilchev†, Leslie Petrik†, Patrick Ndungu‡, and Alexander Nechaev†

*Mechanical and Mechatronics Engineering, Stellenbosch University, South Africa
†Environmental Nanosciences, University of the Western Cape, South Africa
‡Department of Chemistry, University of KwaZulu-Natal, South Africa

ABSTRACT

The effect of decreasing the size of platinum to the nanoscale for the copper-platinum alloy system was investigated while coupled to the research on the electrophoresis of platinum nanoparticles. It was observed that the temperature for the nanoPt-Cu eutectoid transformation decreased to 300°C compared to the value of 418°C for a bulk Pt-Cu system. HRTEM and XRD results showed that sintering between the Pt nanoparticles and copper surface begins at temperatures as low as 200°C. Surface diffusion was dominant at 200°C while bulk diffusion became dominant at 300°C, at which stage the sintered product had formed a tri-phasic system of pure copper, Pt-Cu alloy and Pt nanoparticles which were sintered to the alloy. No platinum nanoparticles remained after sintering at 400°C, having all diffused into the Pt-Cu alloy. Sintering above 300°C saw the appearance of the Cu_3Pt phase. HRTEM imaging of the particles found that there was an increase in particle size from 2.5 nm at 25°C to 0.5 microns at 400°C. These results were compared to particle size calculations using XRD measurements. The particle geometry changed from spherical at 25°C to cubic at and above 300°C.

INTRODUCTION

Nanotechnology is defined as any technology performed on a nanoscale that has applications in the real world.[1] It encompasses any device, natural or synthetic, that has at least one of its dimensions on the length scale of 0.1 – 100 nm. Such devices include thin films, nanolayered materials and membranes (one dimension on the nanoscale), nanotubes, nanorods, nanowires and nanofibres (two dimensions on the nanoscale), as well as nanoparticles, nanospheres, quantum dots, micelles and dendrimers (all three dimensions on the nanoscale.) These are the basic building blocks in nanotechnology and the integration of such components is the basis for the design of nanostructured systems. Perhaps the most exciting discovery in this field was the quantum size effect[1] where as a material's dimensions are reduced to the nanoscale, its properties begin to gradually shift from those of the bulk to novel ones which are better explained by quantum mechanics. Understanding the parameters which control the synthesis outcome and inherent properties of these components allows for the tailoring of novel technological devices which allow the fantastic idea of being able to control chemical systems, on a molecular or even atomic level, to come to life.

The use and development of platinum based materials is becoming ever more crucial in modern technology each day. The application of platinum and its alloys in the field of heterogeneous catalysis is well known and, in many cases, held as a standard. Fuel cell research, as well as other aspects of the hydrogen economy, is mostly based on developing such materials.[2] Additionally, catalytic converters, used to reduce emissions in automobiles and for catalytic cracking in the petroleum industry, have been dependant on platinum alloys since their commercialisation.[3] Other application for platinum in the catalysis industry include the production of chemicals, such as nitric acid[4], hydrogen cyanide[5] and various others hydrocarbons relevant to the petrochemical industry.[6,7]

The selectivity and activity of each process can be modified by using alloys of the different precious metals with each other and/or with other transition metals.[8, 9] Work by both Chandler *et al.*[10] as well as Weihua *et al.*[11] have shown that Pt-Cu bimetallic nanoparticles also show superior catalytic

properties compared to pure platinum. Koh *et al.*[12] and Mani *et al.*[13] both reported on the development of dealloyed Pt-Cu nanoparticles with a near-surface alloy structure as well as a high degree of porosity which not only improved catalyst performance by up to 4 times that of commercial Pt-C but also improved catalyst tolerance to poisoning. Pure platinum has shown poor performance as a catalyst for the oxygen reduction reaction (ORR). The reduction of oxygen in aqueous media by platinum catalysts has been extensively studied for application in fuel cells by Antolini *et al.*[9,14], Bell[15], Luo *et al.*[16,17], Regalbuto[18], Koh *et al.*[12], Mani *et al.*[13] as well as Wang *et al.*[19]. They have shown that binary alloys of platinum with other metals such as cobalt, chromium, vanadium, titanium and copper has shown a marked increase in catalytic activity towards the oxygen reduction reaction.

Van der Biest *et al.*[20] as well as Bersa *et al.*[21] stated that EPD has been successfully employed in the formation of wear-resistant and anti-oxidant coatings, functional films in microelectronic devices and solid oxide fuel cells, membranes, sensors as well as composite and bioactive coatings for medical implants. Teranishi *et al.*[22] prepared 2D nanoarrays of platinum nanoparticles on carbon coated copper grids using EPD. Very little work exists for the EPD of platinum[22-25] hence this research offers insight into possible novel applications for the EPD process of platinum.

By developing a better understanding of the sintering dynamics of the Pt-Cu biphasic system, novel processes for the self-assembly of superior materials of the types mentioned above could be designed. The goal in this research was to determine the effects that reducing the platinum phase to the nanoscale had on the properties of the system.

Abe *et al.*[26] reported that for this system, a eutectoid transformation occurs at 418°C. In theory, reducing either of the phases to the nanoscale would decrease this limit for eutectoid formation. The parameters controlling the formation of CuPt and Cu_3Pt alloys as well as the diffusion characteristics between the Pt and Cu phases was considered by developing a two phase system with a defined boundary between each phase. This was achieved by depositing the platinum nanophase onto a copper foil using electrophoretic deposition (EPD).

EXPERIMENTAL PROCEDURES

Pt Nanoparticle Synthesis and Dispersion

A dispersion of platinum nanoparticles was prepared by the ethylene glycol method[27]. To prepare 200 ml of Pt nanoparticles dispersed in a 1:1 (v/v) mixture of anhydrous acetone and ethanol (AcEt), the following procedure was applied: 1g of NaOH (25 mmol) was dissolved in 50 ml of ethylene glycol (EtGly) at 100°C under N_2. 1g of H_2PtCl_6 (2.44 mmol) was also dissolved in 50 ml of EtGly at room temperature under nitrogen. The two solutions were then mixed together, heated up to 160°C under nitrogen and allowed to react with constant stirring for 2 hours. Once the reaction was complete, 100 ml of ultrapure water was added followed by 25 ml of 1M HCl. The mixture was centrifuged for 30 minutes at 5000 rpm after which the supernatant liquid was discarded. Thereafter, 200 ml of ultrapure water as well as 10 ml of 1M HCl was added to the precipitate, the mixture was shaken well to redisperse the platinum particles. The dispersion was centrifuged again for the same time at the same speed. After centrifugation, the supernatant liquid was discarded again and the platinum precipitate was redispersed in 200 ml of AcEt.

Copper Electrode Preparation

Copper electrodes for the EPD process, with dimensions of 50 mm × 10 mm, were cut from a 5.5 g copper foil of 0.25 mm thickness (supplier: Sigma Aldrich). The copper foil was sanded, sequentially, with 400 grit followed by 600 grit SiC paper,using an active oxide suspension (Struers OP-S suspension), and then polished using cotton wool only, soaked in the suspension. The electrodes were then rinsed with ultrapure water, followed by acetone and finally they were immersed in acetone and sonicated for 15 minutes. The electrodes were then dried with cotton wool.

Electrophoretic Deposition of the Pt Nanoparticles

The EPD apparatus consisted of a DC power supply (supplier: TDK-Lambda, model: Genesys™ GEN600:1.3, 0-600 Volts DC and 0-1.3 Amps DC range, 72 mV and 0.26 mA accuracy) which was connected to a cylindrical brass anode holder and a hollow, cylindrical, stainless steel cathode. The electrodes were housed in a Pyrex container so that the anode rested inside the cathode. Figure 1 shows a schematic diagram of EPD cell.

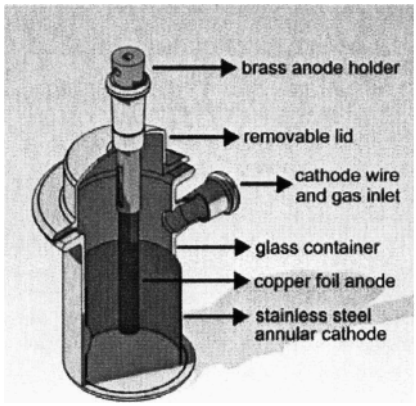

Figure 1. Schematic of the EPD cell.

A set of trials was performed to determine the deposition flux as a function of voltage and deposition time. Each trial was performed in air and 25 ml of the platinum dispersion at a concentration of 1.8 g/l was used. 12 trials with a potential range of 2 – 10 volts and a time range of 5 – 30 minutes were performed to gain an understanding of the deposition kinetics for the system. Table 1 gives the EPD parameters tested.

Table 1 Pt nanoparticle deposition flux at different EPD trial parameters: time at voltage

Deposition time (mins)	Deposition flux (mg/mm^2)		
5	0.0118	0.0210	0.0254
10	0.0150	0.0235	0.0314
20	0.0192	0.0257	0.0327
30	0.0200	0.0259	0.0331
Deposition voltage (V)	2	5	10

To prepare a sample deposit for sintering, 100 ml of the platinum dispersion was diluted with an equal volume of acetone. This dispersion, at a concentration of 0.9 g/l, was then used in the EPD cell to deposit the platinum nanoparticles as a film on the copper foil electrode. The cell was set to an applied voltage of 5 V and deposition occurred for 10 minutes.

Sintering the Pt Deposits

Sintering of the deposits was achieved in a vertical tube furnace. The copper electrode, onto which the Pt nanoparticles had been deposited, was suspended at the mouth of the furnace with a tungsten wire which ran through the furnace. The furnace was heated to the required temperature while being purged by argon gas. The electrode was then hoisted into the furnace with the tungsten wire and kept under flowing argon while the sintering took place. After 15 minutes, the furnace was rapidly purged with argon while the electrode was lowered out of the furnace. Deposit samples were sintered at 100°C, 200°C, 300°C and 400°C.

RESULTS

Synthesis of the Dispersed Pt Nanoparticles

The dispersion prepared was analyzed by HRTEM (high resolution transmission electron microscopy) using a Tecnai F20 field emission transmission electron microscope with coupled EDX (energy dispersive x-ray spectroscopy) capabilities, and XRD (X-ray diffraction) analysis using a PANalytical X'Pert Pro multipurpose diffractomator. The JCPDS (Joint Committee on Powder Diffraction Standards) database was used to characterize the XRD data collected.

The concentration of Pt in dispersion was measured as follows. Three 10 ml samples of the dispersion were each placed in pre-weighed glass vials. The mass of the dispersion in each sample was calculated by weighing the vials after the samples were added. Thereafter, the solvent was evaporated and the vials holding the precipitate only were weighed. The mass of the precipitate multiplied by 100 gives the concentration (in grams per litre) of Pt in the dispersion. The average concentration was taken as the concentration of Pt in the dispersion.

Figure 2(a) shows the HRTEM image of the Pt nanoparticles synthesized by the above procedure and well dispersed in the AcEt solvent mixture. The image shows that the particles are crystalline with an approximate mean particle size of 2 nm. A histogram of the particle size distribution of the dispersed Pt nanoparticles is shown in Figure 2(b). The data was collected by measuring and recording the particles sizes of 51 particles from eight SEM images by hand.

Figure 2(c) shows the XRD pattern for the dispersed Pt nanoparticles. The 2θ peaks of 39.1°, 45.6°, 66.6° and 81.5° in Figure 2(c) are indicative of face centred cubic (fcc) platinum, with the lattice planes for the peaks corresponding to the (111), (200), (220) and (311) planes, respectively. The mean particle diameter, calculated from the XRD spectrum, Figure 2(c), using the Sherrer equation, is 2.2 nm which was in close agreement with the HRTEM results.

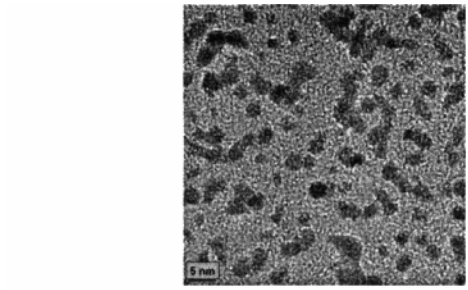

(a)

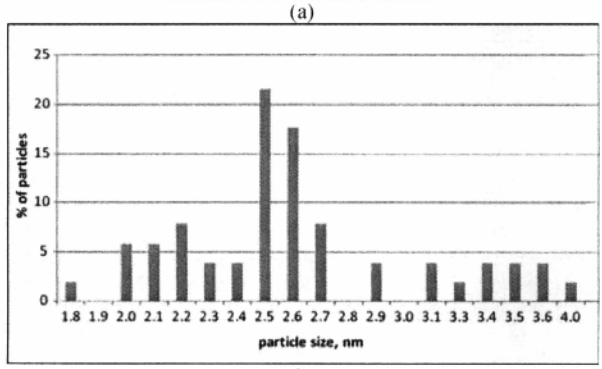

(b)

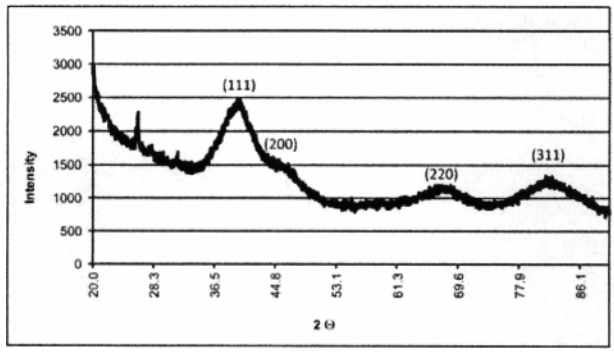

(c)

Figure 2. Imaging and properties of the Pt nanoparticles synthesised: (a) HRTEM image, (b) particle size distribution measured from HRTEM image, and (c) XRD pattern.

EPD of the Pt Nanoparticles onto the Copper Foil Electrodes

The data gathered in the EPD trials was plotted in Figure 3 as deposition flux with respect to deposition time for each applied voltage.

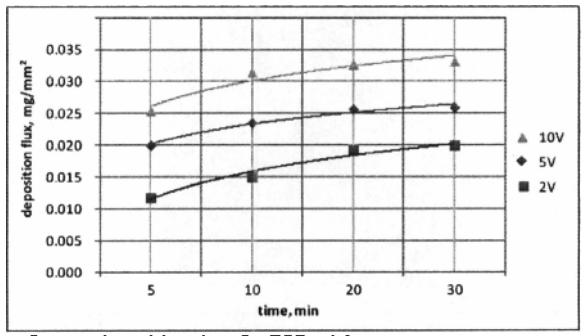

Figure 3. Deposition flux vs. deposition time for EPD trials.

Looking at the graph in Figure 3, the slope of each curve at each applied voltage appears to be similar for all the applied voltages, hence the polarization of the electrode in this system is assumed to be linear for the potential window of 2 – 10 V.

By inspecting the deposits with the naked eye, only the deposits prepared with an applied voltage of 5 V or higher appeared to cover the entire surface of the electrode in contact with the dispersion. Using SEM analysis, performed with a ZEISS EVO MA15VP scanning electron microscope, the thinnest and most uniform film was obtained by running the EPD process at an applied potential of 5 V for 5 minutes. Figure 4(a) shows the SEM image of the deposit prepared on a copper electrode by EPD for 5 minutes at an applied voltage of 5 V. The effect of lowering the dispersion concentration was studied by diluting the dispersion. This was achieved by adding 100 ml of acetone to 100 ml of the prepared dispersion, effectively reducing the Pt concentration in the dispersion to 0.9 g/l. By reducing the amount of ethanol in the solvent mixture as well as the concentration of platinum nanoparticles in dispersion, the deposition flux was further lowered without affecting the uniformity of the deposit significantly, as shown in Figure 4(b). The deposition time was doubled for the diluted dispersion to ensure a continuous platinum film was formed on the copper surface. As the deposition with the diluted dispersion for 10 minutes at 5V gave the best result, these parameters were used to prepare electrodes for the sintering analysis.

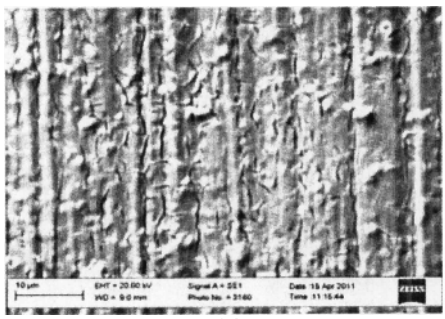

(a)

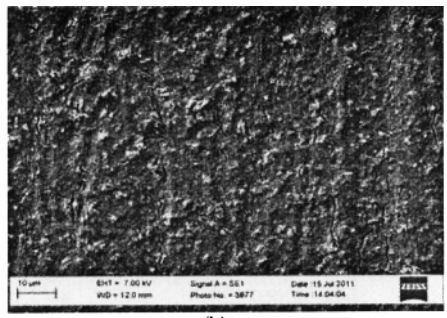

(b)

Figure 4. SEM of Pt deposit on copper electrode after EPD for (a) 5 minutes at 5 V with undiluted dispersion, and for (b) 10 minutes at 5 V with the diluted dispersion.

Sintering of the Pt Deposits

The sintered deposits were analysed by SEM, EDX, XRD, and HRTEM. The microstructure in each of the deposits was investigated using a ZEISS EVO MA15VP scanning electron microscope. Figure 5 shows representative images for each sintered sample.

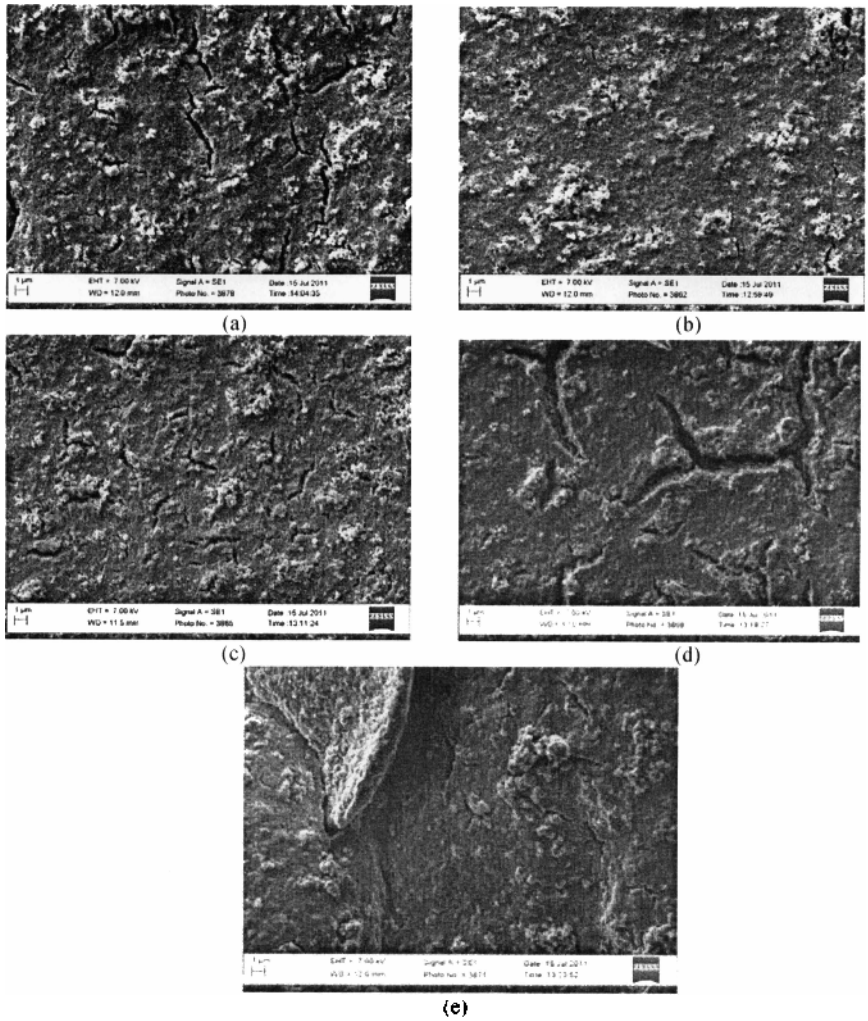

Figure 5. SEM images of Pt deposited on copper electrodes (a) at 25°C, unsintered, and after sintering at (b) 100°C, (c) 200°C, (d) 300°C, and (e) 400°C, in argon for 15 minutes each.

The cracks in the deposit before sintering, as seen in Figure 5(a), disappeared after sintering at 100°C, Figure 5(b), suggesting that the deposited particles were mobile on the copper surface. Both the HRTEM and XRD data indicate no significant change in the mean particle size of the platinum nanoparticles. Table 2 shows the XRD and HRTEM measurements of the mean particle sizes in the deposits.

Table II. XRD and HRTEM measurements of the mean particle size in the deposits

Sintering Temperature (°C)	Mean particle size: HRTEM (nm)	Particle size variation: HRTEM (nm)	Mean particle size: XRD Scherrer (nm)
25	2.5	1.8 - 4.0	2.56
100	2.8	2.0 - 4.0	2.52
200	3.9	2.5 - 5.0	3.96
300	43	2.5 - 150.0	11.72
400	100	10.0 - 600.0	13.83

The XRD spectrum, Figure 6, for the deposit sintered at 100°C also shows that no shift in the d-spacing for the platinum crystal planes has taken place since there is no shift in the 2θ values for the Pt peaks. Hence no alloying between the platinum deposit and the copper electrode had taken place after heating at 100°C.

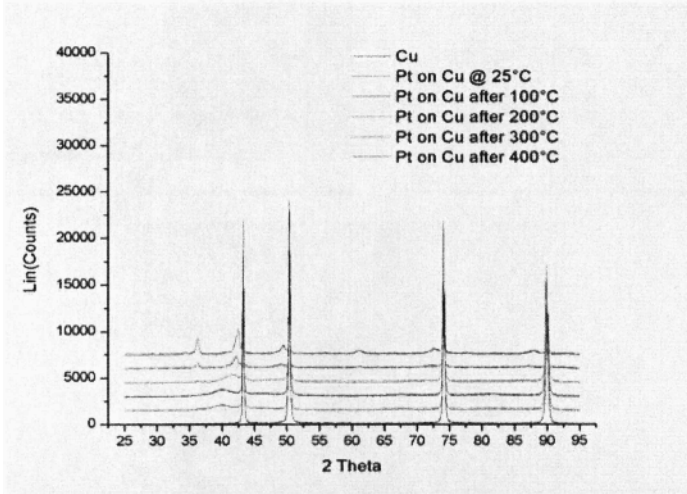

Figure 6. XRD spectra for the copper electrodes as well as the Pt deposits prepared by EPD on the copper electrodes.

HRTEM imaging of the platinum deposit after sintering at 100°C, Figure 7(b), indicates that no necking between the platinum nanoparticles had occurred at 100°C. Therefore, it can be concluded that no significant surface diffusion was taking place between the particles. The disappearance of the cracks

in the deposit can be attributed to settling of the Pt nanoparticles as the residual solvent and water evaporated from the deposit.

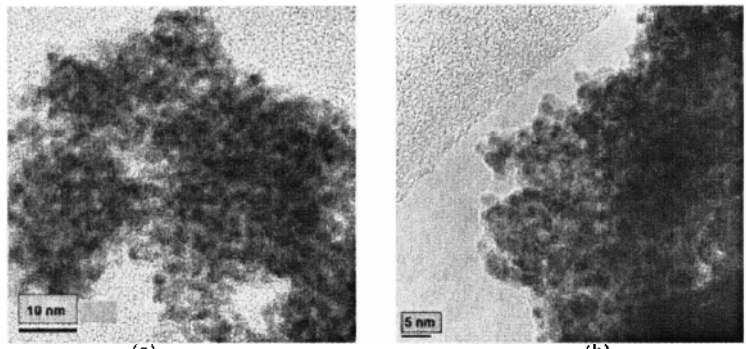

(a) (b)

Figure 7. HRTEM image of Pt deposit scraped off the copper electrode (a) before sintering, and (b) after sintering at 100°C.

Fine cracks reappeared on the deposit surface after sintering at 200°C, shown in Figure 5(c). This was indicated the formation of a densification gradient between the deposit and the copper surface, as well as immobilization of the deposit due to bonding with the copper substrate. In other words, sintering of the platinum nanoparticles must have begun at this temperature. Furthermore, the shift in the 2θ value for the [111] peak in the XRD spectrum of the platinum deposit from 40.0° to 41.6° is indicative of a decrease in the d-spacing of the [111] planes for the platinum phase indicating the onset of alloying. The other peaks had signals which were too weak to be detected. The mean particle size from both the XRD and HRTEM data, Figure 6 and Figure 8(a), was calculated to be 3.9 nm in both cases, indicating that very little coarsening had occurred. Densification of the deposit was occurring dominantly via surface diffusion at this temperature.

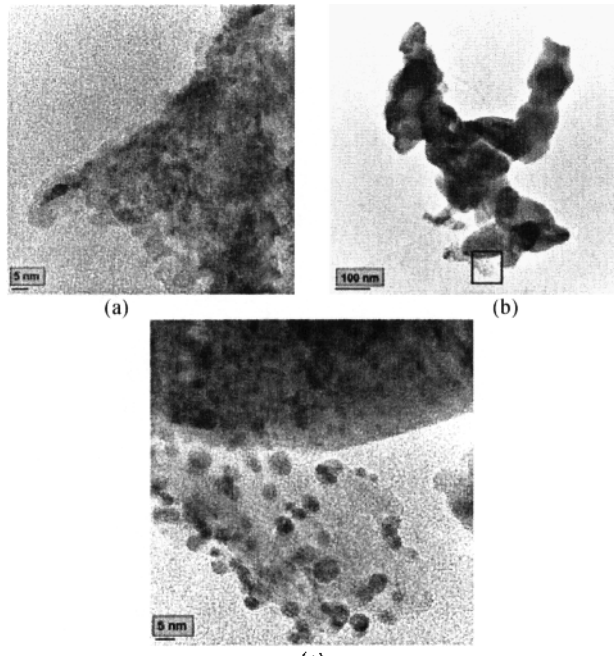

(a) (b)

(c)

Figure 8. HRTEM image of Pt deposit after sintering at (a) 200°C, and (b) 300°C, with magnified imaging of the area in the block shown in (c).

After sintering at 300°C, both HRTEM imaging, Figure 8 (b) and (c), and XRD analysis, Figure 6, unambiguously indicate both sintering as well as alloying between the Pt nanoparticles and the Cu surface. The HRTEM images show significant particle growth as well as distinct necking between the particles. Upon closer inspection, Figure 8(c), the surface of most of the sintered particles is dispersed with pure platinum nanoparticles, which are sintered to the main alloy. The XRD spectrum for this deposit sample showed a further increase in the 2θ value for the [111] peak from 41.62° to 42.22°, closer to the peak characteristic of the Cu_3Pt phase. The peak intensities also rose, indicating an increase in the amount of alloy forming. The [200] peak was now also visible. The peaks at 2θ = 36.2° and 61.0° are characteristic for the [111] and [220] peaks, respectively, for Cu_2O. This suggested that either some oxygen was being introduced into the furnace during sintering or that some organic stabilizing agents on the Pt nanoparticles in the dispersion, such as glycolate ions, were being retained in the deposit and were reacting with the deposit at 300°C to release oxygen. Due to the low concentration of Cu_2O that had formed, no HRTEM images of its presence in the deposits could be taken.

At this point, a triphasic system had formed including the pure copper substrate, sintered Pt-Cu alloy and the unsintered Pt nanoparticles. Here, the correlation between the mean particle size calculated using the HRTEM and XRD data was lost. This was due to the peak overlap between the Pt and Cu_3Pt peaks in the XRD spectrum, i.e. the Cu_3Pt peaks were interfering with the much less intense

Pt peaks, hence the mean particle size of the Pt nanoparticles on the Pt-Cu alloy could not be calculated from the XRD data for that sample. The polycrystalline nature of the eutectoid formation was another factor which led to the Scherrer equation for the XRD data for the sample sintered at 300°C effectively calculating the mean grain size of the Pt-Cu eutectoid phase. Looking at the trend for the variation in particle size for each deposit, shown in Table 2, it is confirmed that sintering at temperatures of 300°C and above causes a loss in the correlation between the calculated values for the mean particle sizes of the samples when using HRTEM and XRD data. The HRTEM data is considered less ambiguous for such multiphasic systems, though it is more tedious to analyse. The XRD data is still useful in predicting the size of the grains in a polycrystalline solid. The small size of the grains for the samples sintered at 300°C and 400°C is characteristic of a rapidly cooled eutectoid.

Figure 9 shows an HRTEM image of the Pt deposit after sintering at 400°C. Compared to Figure 8(a) and 8(b), it shows that the deposit has sintered to the point where the previous particle boundaries are no longer apparent and the deposit now appears as a continuous film. There is no indication of discrete Pt nanoparticles on the deposit surface, as was the case in Figure 8(c). Table III gives the EDX analysis on the deposit surface measured at several points, reported as the average of the measurements. There is no pure Pt present at any of the points analysed. It is surmised that the Pt has diffused below the surface, alloying with the Cu substrate at subsurface level.

XRD analysis, Figure 6, indicated that the most prominent alloy within the nanoparticle structures was Cu_3Pt. It also indicated that the amount of Cu_2O in the sample increased.

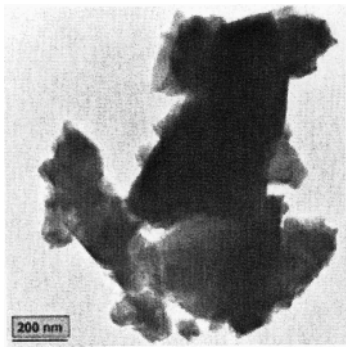

Figure 9. HRTEM images of Pt deposit scraped off the copper electrode after sintering at 400°C.

Table III. EDX data for the deposit sintered at 400°C

Element	Weight %	Atomic %	Uncert. %	Detector correction	k-factor
C(K)	9.10	26.25	0.12	0.26	3.94
O(K)	14.74	31.90	0.11	0.49	1.974
Ni(K)	7.81	4.61	0.07	0.99	1.511
Cu(K)	68.33	37.23	0.20	0.99	1.667
Pt(L)	0.00	0.00	100	0.75	5.547

A change in the particle geometry from spherical at 25°C to mostly cubic was noted to begin at 300°C and it became more pronounced at 400°C, as can be seen in Figure 9. This suggested that the Cu_3Pt system favours growth of the [100] crystal face. This deduction was in contradiction to the XRD

results which showed a higher diffraction intensity for the lower surface energy inducing [111] crystal planes. This suggests that a different crystal structure exists at the deposit surface compared to the subsurface level. If a temperature gradient had forms from the deposit surface down, then crystal growth would be kinetically favoured at the surface, where the phase transformation was more rapid, resulting in the formation of the less kinetically hindered [100] crystal faces. These faces also contain fewer platinum atoms than the [100] crystal planes, meaning that they would be more thermodynamically feasible to form at the surface during the diffusion of the Pt into the Cu substrate. Similar behaviour has been reported for Pt evaporated onto a Cu single crystal [111] face and heated above 500 K (227°C).[28] For contrasting reasons, the subsurface level would have grains more randomly oriented, with the most thermodynamically stable [111] planes being the predominant grain boundaries. The high magnification HRTEM image of the sample sintered at 400°C, Figure 10, shows the lattice fringes within the sample indicating the formation of a polycrystalline phase.

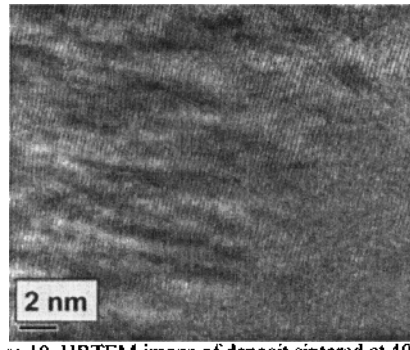

Figure 10. HRTEM image of deposit sintered at 400°C.

CONCLUSIONS AND FUTURE WORK

This research demonstrated that Pt nanoparticles with a narrow particle size distribution are formed easily and remain in dispersion indefinitely when prepared by the ethylene glycol synthesis method. The dispersions prepared were also stable throughout the timeline of the research. It was also demonstrated that the EPD process can be applied to the dispersions of Pt nanoparticles even in a low electrolyte media, though a small amount of reactive solvent or redox initiator aids in the EPD kinetics, as does the polarizability of the electrode surface. It was confirmed that the dynamics of the EPD process were retained in the setup used and deposits with various densities, thicknesses and coherencies could be prepared by only altering the EPD parameters, applied potential, deposition time and dispersion concentration. By developing the EPD process a better control of the deposit density, thickness and coherency can be obtained. Factors such as the solvent composition, use of stabilizing agents and particle concentrations should all be looked into for improving the versatility of the process. Sintering of the platinum deposit was achieved at low temperatures compared to typical bulk platinum sintering temperatures. The eutectoid transformation, typically occurring at 418°C for bulk Pt-Cu alloys, occurred at a reduced temperature, around 300°C, for Pt nanoparticles sintered to a Cu substrate. The sintering kinetics were slow at 200°C, due to the copper existing as a bulk phase, hence sintering occurred dominantly via surface diffusion, and little Cu-Pt alloy formation occurred. The triphasic deposit, formed after sintering at 300°C, could be considered for a heterogeneous catalyst system due to the fine dispersion of platinum on the eutectic surface. Work on the sintering dynamics, through optimization of the sintering times as well as heating rates and cooling rates, could aid in improving

this procedure to compete with current state of the art synthesis methods for catalysts and hard disk platters. Determining whether the oxygen responsible for the Cu_2O formation came from the atmosphere or from occluded organic impurities in the deposit needs to be determined and circumvented in order to ensure purity of the structures formed by this procedure. While most of the work in this article was conceptual, testing the sensitivity of this system to scaling up should be considered as the procedures used in this research are relatively inexpensive.

ACKNOWLEDGEMENTS

This work was presented at The International Conference on Sintering 2011, 28 August – 2 September 2011, Jeju, Korea. It was funded by the National Research Foundation (South Africa) under their Nanotechnology Flagship Programme, Project "Nano-architecture in the beneficiation of platinum group metals."

REFERENCES

[1] B. Bhushan, Springer Handbook of Nanotechnology, Springer, USA (2004).
[2] J. Rifkin, The Hydrogen Economy: The Creation of the Worldwide Energy Web and the Redistribution of Power on Earth. J.P. Tarcher/Putnam, USA (2002).
[3] S.T. Gulati, New Developments in Catalytic Converter Durability, *Studies in Surface Science and Catalysis* **71**, 481-507 (1991).
[4] W. Ostwald, Improvements in the Manufacture of Nitric Acid and Nitrogen Oxides, *Patent GB 190200698(A)* (1902).
[5] R.J.H. Voorhoeve, C.K.N. Patel, L.E. Trimble, and R.J. Kerl, Hydrogen Cyanide Production During Reduction of Nitric Oxide over Platinum Catalysts: Transient Effects, *Science*, **200**, 761-763 (1978).
[6] J.G. Speight, Synthetic fuels handbook: properties, process, and performance, McGraw-Hill Professional, USA (2008).
[7] N.H. Sager, and R.M.L. Pouteau, The Production of Heavy Water: Hydrogen-Water Deuterium Exchange Over Platinum Metals on Carbon Supports, *Platinum Metals Rev.*, **19** (1), 16-21 (1975).
[8] S. Nishimura, Handbook of heterogeneous catalytic hydrogenation for organic synthesis, J. Wiley, USA (2001).
[9] E. Antolini, Platinum-based ternary catalysts for low temperature fuel cells Part I. Preparation methods and structural characteristics, *Applied Catalysis B: Environmental*, **74**, 324-336 (2007).
[10] B.D. Chandler, A.B. Schabel, L.H. Pignolet, Preparation and Characterization of Supported Bimetallic Pt-Au and Pt-Cu Catalysts from Bimetallic Molecular Precursors., *J. Catal.*, **193** (2), 186-198 (2000).
[11] W. Weihua, T. Xuelin, C. Kai, and C. Gengyu, Synthesis and characterization of Pt–Cu bimetallic alloy nanoparticles by reverse micelles method, *Colloids and Surfaces A: Physicochem. Eng. Aspects*, **273**, 35-42 (2006).
[12] S. Koh, and P. Strasser, Electrocatalysis on bimetallic surfaces: modifying catalytic reactivity for oxygen reduction by voltammetric surface dealloying, *J Am Chem Soc.*, **129**, 12624-12625 (2007).
[13] P. Mani, R. Srivastava, and P. Strasser, Dealloyed Pt–Cu Core–Shell Nanoparticle Electrocatalysts for Use in PEM Fuel Cell Cathodes, *J. Phys. Chem. C*, **112**, 2770-2778 (2008).
[14] E. Antolini, R.R. Passos, and E.A. Ticianelli, Electrocatalysis of oxygen reduction on a carbon supported platinum–vanadium alloy in polymer electrolyte fuel cells, *Electrochimica Acta*, **48**, 263-270 (2002).
[15] A.T. Bell, Catalysis looks to the future. National Academies Press, USA, (1992).
[16] J. Luo, L. Han, N. Kariuki, L. Wang, D. Mott, C.J. Zhong, and T. He, Synthesis and Characterization of Monolayer-Capped PtVFe Nanoparticles with Controllable Sizes and Composition, *Chem. Mater.*, **17**, 5282-5290 (2005).

[17] J. Luo, L. Wang, D. Mott, P.N. Njoki, N. Kariuki, C.J. Zhong, and T. He, Ternary alloy nanoparticles with controllable sizes and composition and electrocatalytic activity, *J. Mater. Chem.*, **16**, 1665-1673 (2006).
[18] J.R. Regalbuto, Catalyst preparation: Science and Engineering, CRC Press, USA (2006).
[19] Y. Wang, J. Ren, K. Deng, L. Gui, and Y. Tang, Preparation of Tractable Platinum, Rhodium, and Ruthenium Nanoclusters with Small Particle Size in Organic Media, *Chem. Mater.*, **12**, 1622-1627 (2000).
[20] O.O. Van der Biest, and L.J. Vandeperre, Electrophoretic Deposition of Materials, *Annu. Rev. Mater. Sci.*, **29**, 327-352 (1999).
[21] L. Besra, and M. Liu, A review on fundamentals and applications of electrophoretic deposition (EPD), *Progress in Materials Science*, **52**, 1-61 (2007).
[22] T. Teranishi, M. Miyake, and M. Hosoe, Formation of Monodispersed Ultrafine Platinum Particles and their Electrophoretic Deposition on Electrodes, *Adv. Mat.*, **9** (1), 65-67 (1997).
[23] T. Teranishi, M. Hosoe, T. Tanaka, and M. Miyake, Size Control of Monodispersed Pt Nanoparticles and Their 2D Organization by Electrophoretic Deposition, *J. Phys. Chem. B*, **103**, 3818-3827 (1999).
[24] X. Yin, Z. Xue, and B. Liu, Electrophoretic deposition of Pt nanoparticles on plastic substrates as counter electrode for flexible dye-sensitized solar cells, *J. Power Sources* **196** (4), 2422-2426 (2011).
[25] J.S. Zheng, M.X. Wang, X.S. Zhang, Y.X. Wu, P. Li, X.G. Zhou, and W.K. Yuan, Platinum/Carbon Nanofiber Nanocomposite Synthesized by Electrophoretic Deposition as Electrocatalyst for Oxygen Reduction, *J. Power Sources*, **175** (1), 211-216 (2008).
[26] T. Abe, B. Sundman, and H. Onodera, Thermodynamic Assessment of the Cu-Pt System, *J. Phase Equilibria and Diff.*, **27**(1), 5-13 (2006).
[27] A. Ilchev, Platinum group alloy nanoparticle architecture and their electrophoretic deposition, MSc thesis, University of the Western Cape, South Africa (2011).
[28] U. Schröder, R. Linke, J-H. Boo, and K. Wander, Adsorption properties and formation of Pt/Cu surface alloys, *Surface Sci.*, **352-354**, 211-217 (1996).